Supporting Information

Zwitterion Functionalized Carbon Nanotube/Polyamide Nanocomposite Membranes for Water Desalination

Wai-Fong Chan[a,*], *Hang-yan Chen*[b,*], *Anil Surapathi*[a], *Michael G. Taylor*[b], *Xiaohong Shao*[c], *Eva Marand*[a,†] *and J. Karl Johnson*[b,d,‡]

[a]Department of Chemical Engineering, Virginia Polytechnic Institute and State University, 138 Randolph Hall, Blacksburg, VA 24061, USA

[b]Department of Chemical & Petroleum Engineering, University of Pittsburgh, 15261 Benedum Hall, Pittsburgh, PA, 15213, USA

[c]College of Science, Beijing University of Chemical Technology, Beijing 100029, People's Republic of China

[d]National Energy Technology Laboratory, Pittsburgh, PA, 15236, USA

[*]These authors contributed equally

[†]emarand@vt.edu

[‡]karlj@pitt.edu

Membrane Fabrication. The interfacial polymerization (IP) of polyamide (PA) is very sensitive to the operating condition and reaction time. Moreover, there are many ways to carry out the procedure. Different publications report different recipes in terms of the concentration of monomers, contact time, air-drying time, curing temperature, etc.[1-4] A schematic of our recommended fabrication procedure is shown in Figure 8. The polyethersulfone PES membrane support was first pretreated by soaking in a 0.5 wt% sodium dodecylbenzenesulfonate (SDBS) solution (Figure 8A) for two days to increase the hydrophilicity and to open the pores of the support. The support was then soaked in deionized (DI) water for one day to remove any excess surfactants. This soaking pretreatment guaranteed that there was no SBDS solution left in the pores. The absence of this step may introduce air bubbles underneath the later PA layer. The support was then sandwiched in between two round Poly(tetrafluoroethylene) (PTFE) holders. Before being poured on the top of the membrane support, a predetermined weight of zwitterion-functionalized CNTs was dispersed in 40 ml of deionized (DI) water by sonication. During the sonication step, the CNT solution was heated by the sonicator horn and therefore required cooling to room temperature. As shown in Figure 8, the functionalized CNTs were deposited and semi-aligned on the membrane support using high-vacuum filtration.[5] The support and CNTs were then dried for an hour in a vacuum oven. This insured that all water was removed from the nanotubes before the interfacial polymerization took place. An alternative way to filter the CNT solution was to use a solvent-resistant stirred cell (XFUF04701; Millipore, MA). This apparatus utilized a dead-end filtration method, in which the support was held at the bottom of the cell and the CNTs solution was stored within the cell above the support. The cell was pressurized up to 6 bar with inert gas on the top of the solution. Under this relatively high pressure the CNT solution also filtered through the support leaving the CNT behind. As shown in Figure 8C, IP was subsequently carried out on the CNT covered support by wetting the fabrication side (with CNTs) with an aqueous diamine solution containing 2 wt% MPD and 0.2 wt% of SDBS at ambient temperature for 2 min and then the membrane was unclamped and immediately placed on a glass plate. A glass roller was rolled over the membrane once to remove all the excess MPD solution. The membrane was then sandwiched again into the holder and wetted by a n-hexane solution containing 0.5% (w/v) TMC for 90 seconds. The resulting PA thin film nanocomposite membrane was subsequently heat cured at 68°C for 5 min. After the membrane had cooled down, it was washed thoroughly with DI water, submersed in fresh DI water and stored in a laboratory refrigerator at 4°C. The thickness and diameter of the interfacial PA layer (Figure 8D) was approximately 500 nm and 3.7 cm, respectively. [6, 7]

CNT Characterization. The surfaces and cross-section of the membranes were characterized by field emission scanning electron microscopy (FESEM, LEO 1550). Membrane samples were prepared for SEM cross-section imaging by gently peeling away the polyester backing fabric to ensure PES and Z-CNTs/PA layers remained together. A small piece of fabric-free membrane sample was frozen in liquid nitrogen and fractured cryogenically. The surface morphologies of the PES support, PA and Z-CNTs/PA nanocomposite membranes were studied using FESEM and images are shown in Figure S3, parts A, B, and C, respectively. The cross-sectional view of the Z-CNTs/PA membrane, also taken by FESEM, is shown in Figure S3-D. The neat PES support (Figure S3-A) has a relatively smooth and porous surface with pore sizes ranging approximately from 6 to 20 nm. After interfacial polymerization, a thin PA skin layer with ridge-valley shape was formed on the top of the PES substrate (Figure S3-B) and acted as a barrier layer in separating salt ions from water. For the Z-CNTs/PA nanocomposite membrane (Figure

S3-C), we see that all the nanotubes were covered by interfacially polymerized PA. Due to the random packing of Z-CNTs, the surface roughness of the nanocomposite membrane is greatly increased relative to plain PA. The cross-section of the Z-CNTs/PA membrane (Figure S3-D) shows that nanotubes are embedded in PA with semi-aligned orientation (examples indicated by arrows).

Zwitterion Charge Fitting. Atom-centered charges for the zwitterions were obtained by computing the electrostatic potential of a zwitterion attached to the end of a (20,0) CNT within density functional theory. We used the Perdew-Burke-Ernzenhof generalized gradient approximation functional[8] as implemented within the Vienna Ab Initio Simulation Package.[9-12] An energy cutoff of 520 eV was used in the calculations. The resulting electrostatic potential was then fitted to point charges using the method of Chen et al.[13] The resulting charges where then normalized so that the overall charge on the zwitterion was zero. This was needed because there were atom-centered charges on the carbon atoms of the nanotube, in addition to the zwitterion. However, the charges on the nanotube atoms were small in magnitude, so that the renormalization of the zwitterion charges made only minor changes to the computed values.

Estimation of Flow Rate Error Bars. The standard deviations for the flow rate calculations, shown in Table 1, were computed using block averages of the simulation data. The linear least squares method was used to fit a line to each block of data to get the flow rate (molecules/CNT/ns) in each block. The standard deviation was calculated from $\sigma = \sqrt{\frac{(J-\bar{J})^2}{n-1}}$, where J is the flux of ions or water, and n represents the number of blocks. The errors in the ion rejection ratios were calculated by $1-\frac{J_{ion}+\sigma_{ion}}{J_{water}-\sigma_{water}}\times\frac{C_{water}}{C_{ion}} < R < 1-\frac{J_{ion}-\sigma_{ion}}{J_{water}+\sigma_{water}}\times\frac{C_{water}}{C_{ion}}$, where σ_{ion} and σ_{water} represent the standard deviations of the conductance of ions and water.

Estimation of Flux Through an Ideal Membrane. In an ideal membrane all water flux will be through the carbon nanotubes and no water or ions would permeate through the polymer matrix. All the nanotubes would be semi-aligned so that they provided a pathway from one side of the membrane to the other. Taking the experimental membrane having 20 wt% (0.75 mg) CNTs, and assuming a nominal (20,0) CNT as the average nanotube having a length of 1000 nm, we can compute the average number of CNTs per membrane. The diameter of the membrane is 3.7 cm, so that the total area is 10.75 cm^2. This membrane would have a density of 1.86×10^{13} CNT/cm^2. Assuming a linear flux of water with pressure drop,[14] we get a flux of 1.75 water molecules per CNT per ns. Converting to units of gallons per square foot per day gives a flux of about 20,000 GFD at a pressure drop of 530 psi.

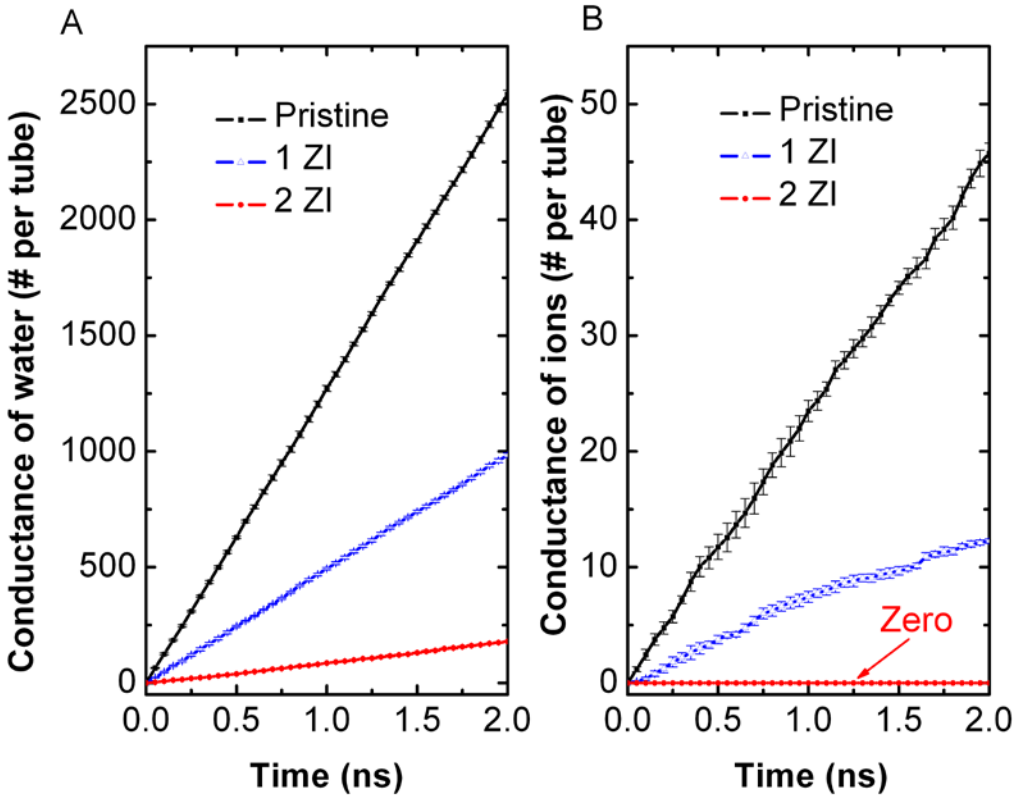

Figure S1. Conductance of (A) water and (B) ions per CNT for pristine (non-functionalized) nanotubes (black line with solid squre), CNTs with one zwitterion (1 ZI) at each end (blue line with empty triangle), and with two zwitterions (2 ZI) at each end (red line with solid circle) for a bulk concentration of 0.6 M KCl and a pressure drop of 208 MPa. Error bars show the standard deviation based on four independent simulations.

Estimation the Number of Zwitterions per CNT. In the experiment, the average diameter of CNTs is about 15 Å, close to the diameter of a CNT (20,0) which is 15.66 Å. Thus, we consider the (20,0) CNT in the estimation of the number of zwitterions per CNT. In a CNT with indices (*n*,*m*), the length of one unit cell is calculated as $L = \frac{\sqrt{3}\pi d_{cnt}}{d_R}$,[15] where d_R is the common divisor for (2*n*+*m*, 2*m*+*n*) and d_{cnt} is the diameter of a CNT. For a (20,0) CNT, L is given as 4.26 Å. The number of atoms in one unit cell of a CNT is calculated as $n_c = \frac{4(n^2+m^2+n\times m)}{d_R}$.[15] Thus, in a (20,0) CNT, the number of atoms per unit cell is 80. The length of the CNTs used in experiments is around 1 μm, so that the number of C atoms in one CNT is $\frac{80}{0.426\text{nm}} \times 1000\text{nm} = 1.88\times10^5$ C atoms/CNT. The atomic percentages of C and N in zwitterion functionalized CNTs were measured by x-ray photoelectron spectroscopy. The results show that for every 100 atoms of the

sample, 77 are C atoms and 2 are N atoms. Zwitterion groups we used have the structure: -COO-$(CH_2)_3$-$N^+(CH_3)_2$-$(CH_2)_2$COO-. Thus, each zwitterion group has one nitrogen atom and hence there are 2 zwitterion groups per 77 carbon atoms. For 77 carbon atoms, 18 of them are carbon atoms contained in the zwitterion groups. Let the number of zwitterion groups in a typical CNT be *x*. Using proportionality, *x* is calculated as $\frac{77-18}{2} = 29.5 = \frac{1.88\times10^5}{x}$. Therefore, the number of zwitterions is estimated to be 6400 per CNT. Given that there are only 20 dangling bonds at each end of a (20,0) CNT, the maximun number of zwitterions attached at the ends is 40. Thus, most of zwitterions must be bound to the tube wall, presumably at defect sites along the length of the nanotube.

Weighted Histogram Analysis. The initial configuration for each window before the sampling is an equilibrated state. In order to reach that equilibrated configuration, we performed two simulation steps before sampling. Firstly, starting from one configuration with the sampled carbon atom located in the interior of the pore, the sampled carbon atom was moved to the center of the target window by applying a one dimensional spring $U=k_z(z-z_0)^2$ with force constant of k_z=50 kcal/mol/Å^2 to the sampled carbon atom for a short MD run of 100 ps. Secondly, the system was equilibrated with the same spring potential for 500 ps to ensure that the sampled atom was located near the center of the window. Next, we started the sampling by using a one dimensional spring with a force constant of 1 kcal/mol/Å^2. The sampling process lasted for 500 ps. The initial 100 ps was discarded and only the last 400 ps was used for the WHAM analysis.

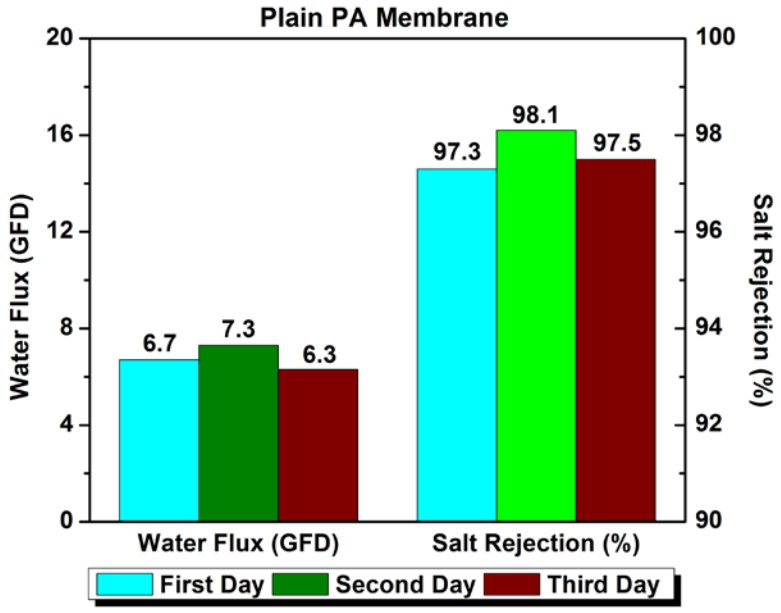
Plain PA Membrane
Water Flux (GFD)
Salt Rejection (%)
6.7
7.3
6.3
97.3
98.1
97.5
Water Flux (GFD)
Salt Rejection (%)
First Day
Second Day
Third Day

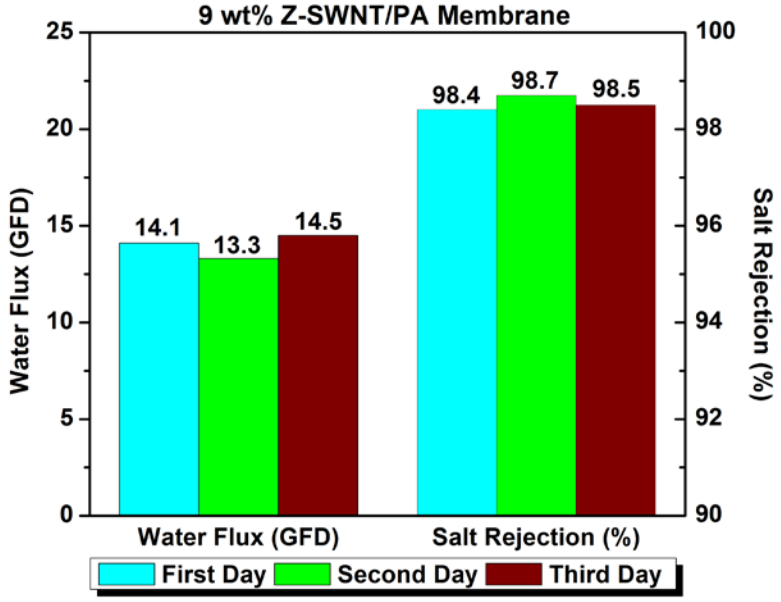
9 wt% Z-SWNT/PA Membrane
Water Flux (GFD)
Salt Rejection (%)
14.1
13.3
14.5
98.4
98.7
98.5
Water Flux (GFD)
Salt Rejection (%)
First Day
Second Day
Third Day

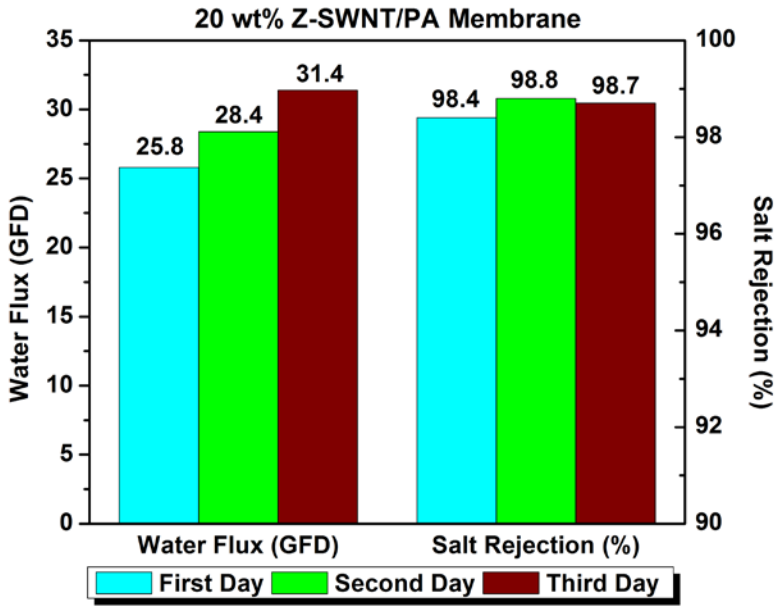

Figure S2. Water flux and salt rejection for pure PA membrane 9 wt% Z-SWNT/PA and 20 wt% Z-SWNT/PA membrane operated for a pressure drop of 530 psi.

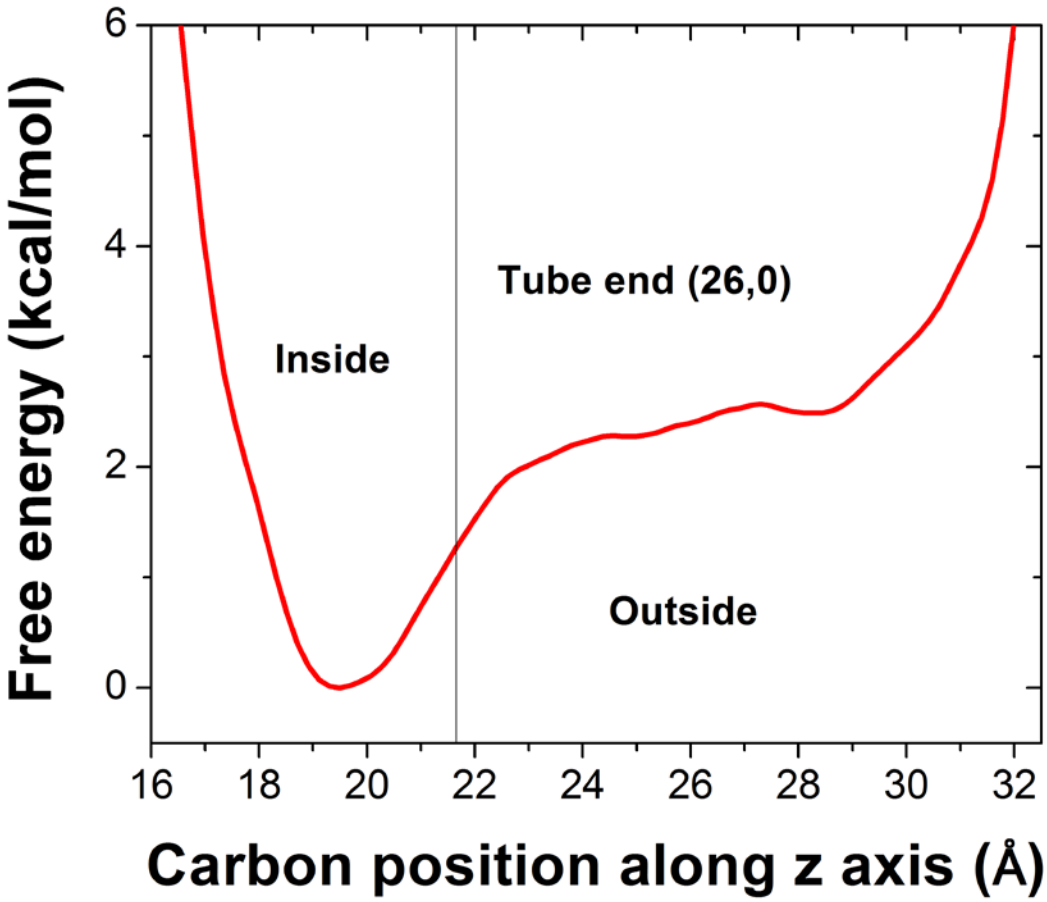

Figure S3. PMF for moving five zwitterions from inside (folded) to outside (unfolded) of a (26,0) CNT as a function of the zwitterion terminal carbon atom position.

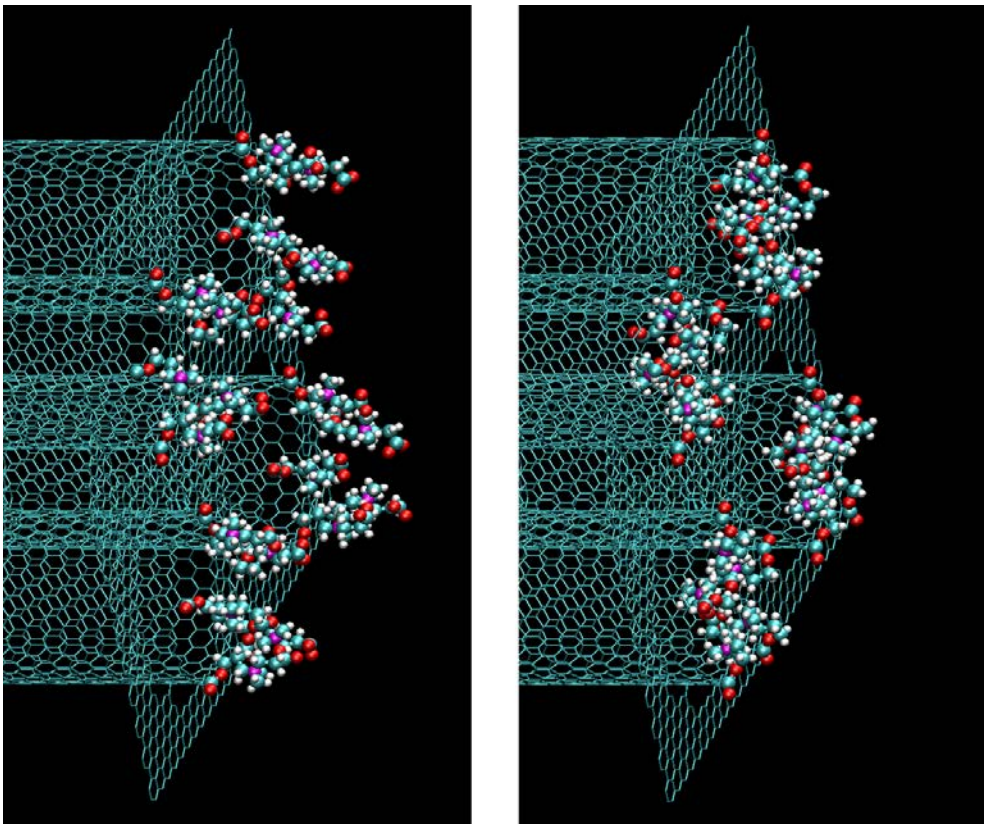

Figure S4. Initial (left panel) and final (right panel) configurations of a 4 ns simulation of 0.6 M NaCl in contact with a membrane having five zwitterions on the ends of each of the four (26,0) CNTs. For clarity, the water molecules and salt ions are not shown.

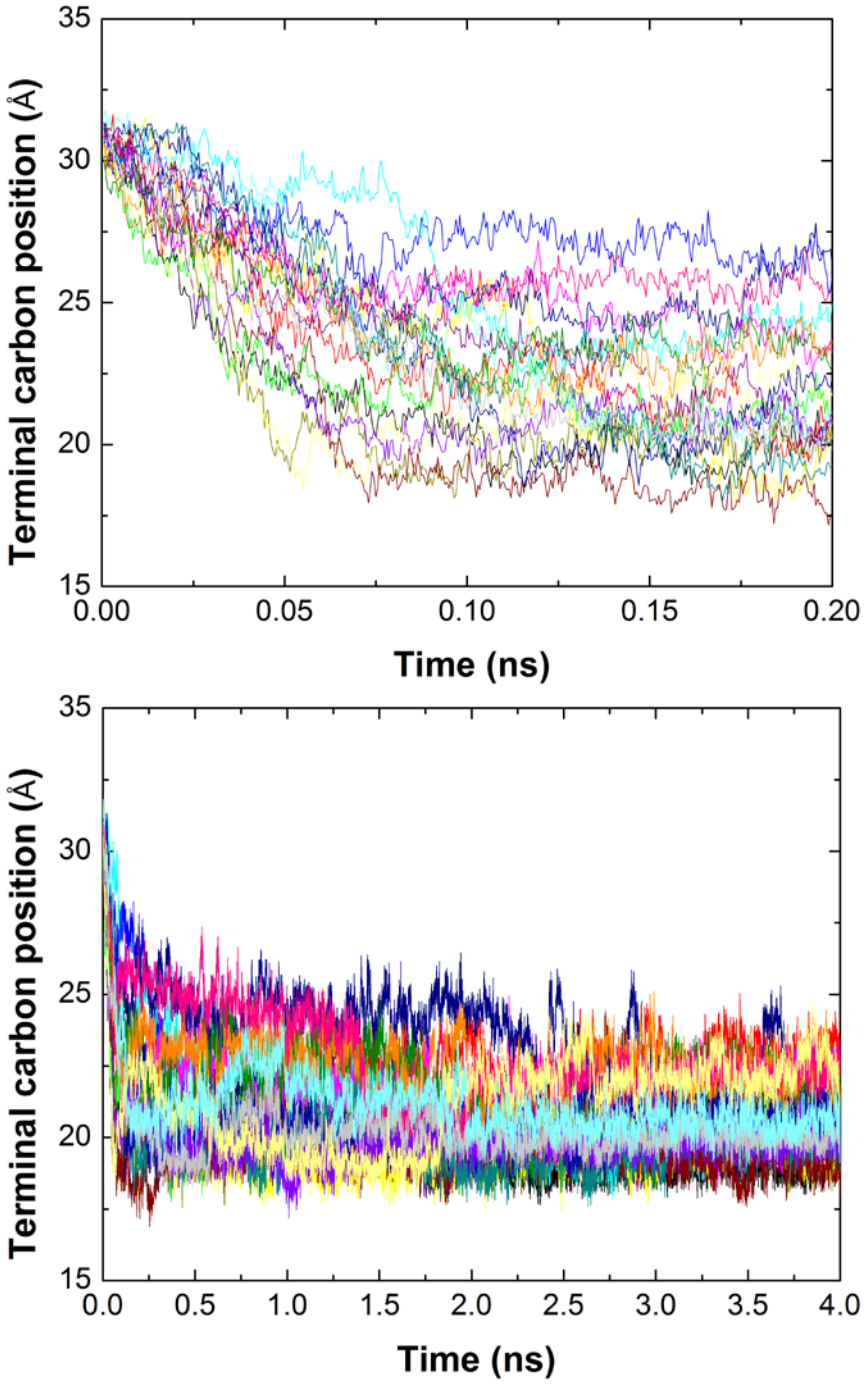

Figure S5. Positions of the 20 terminal carbons on the zwitterions at the ends of the nanotubes shown in Figure S4 as a function of time. Top panel shows the initial 0.2 ns of the simulation and the bottom panel shows the full 4 ns simulation time. Note that at the end of the simulation that all terminal carbons are below a distance of 25 Å, with most lying below 22 Å, which may be considered folded configurations.

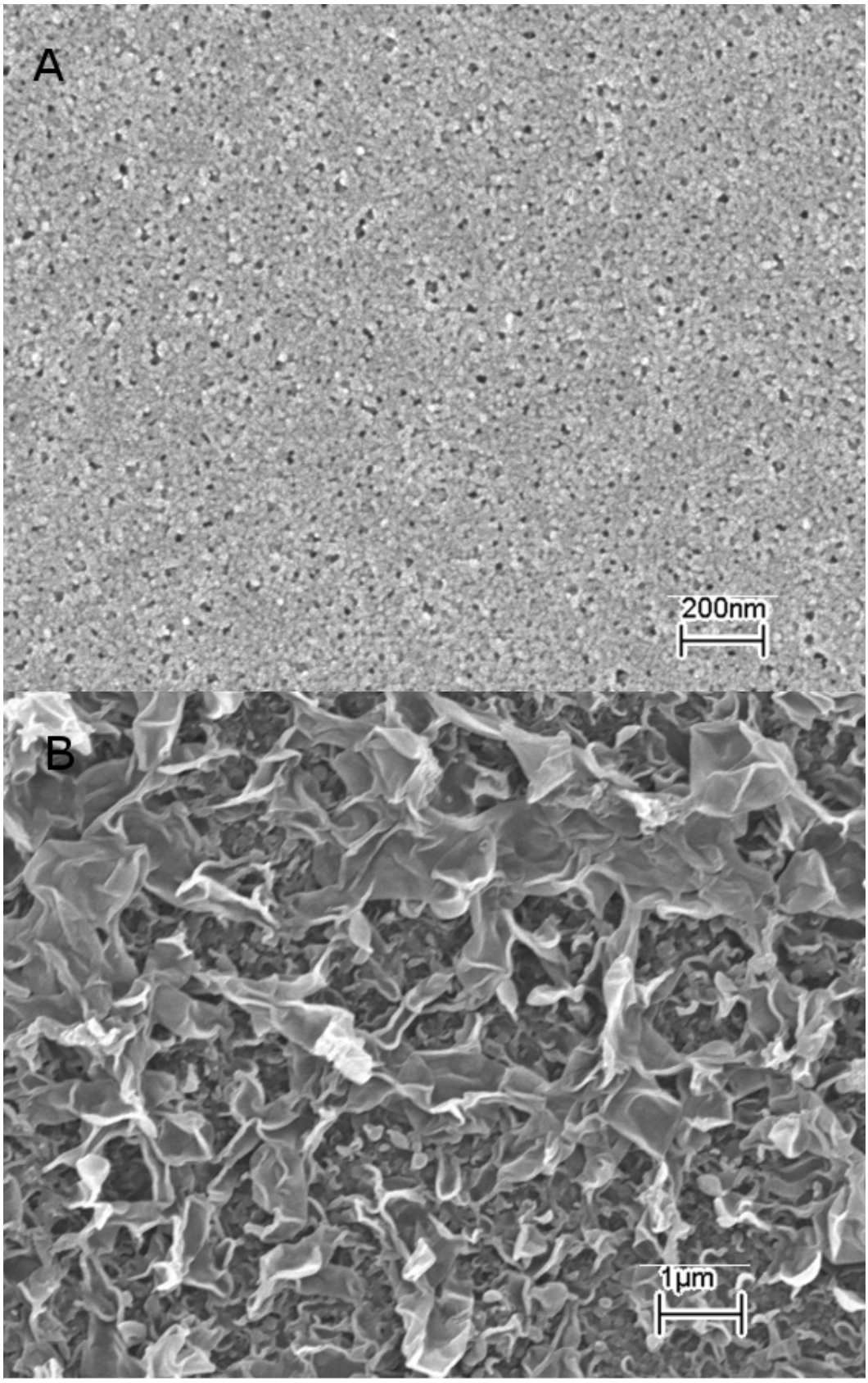
A
200nm
B
1μm

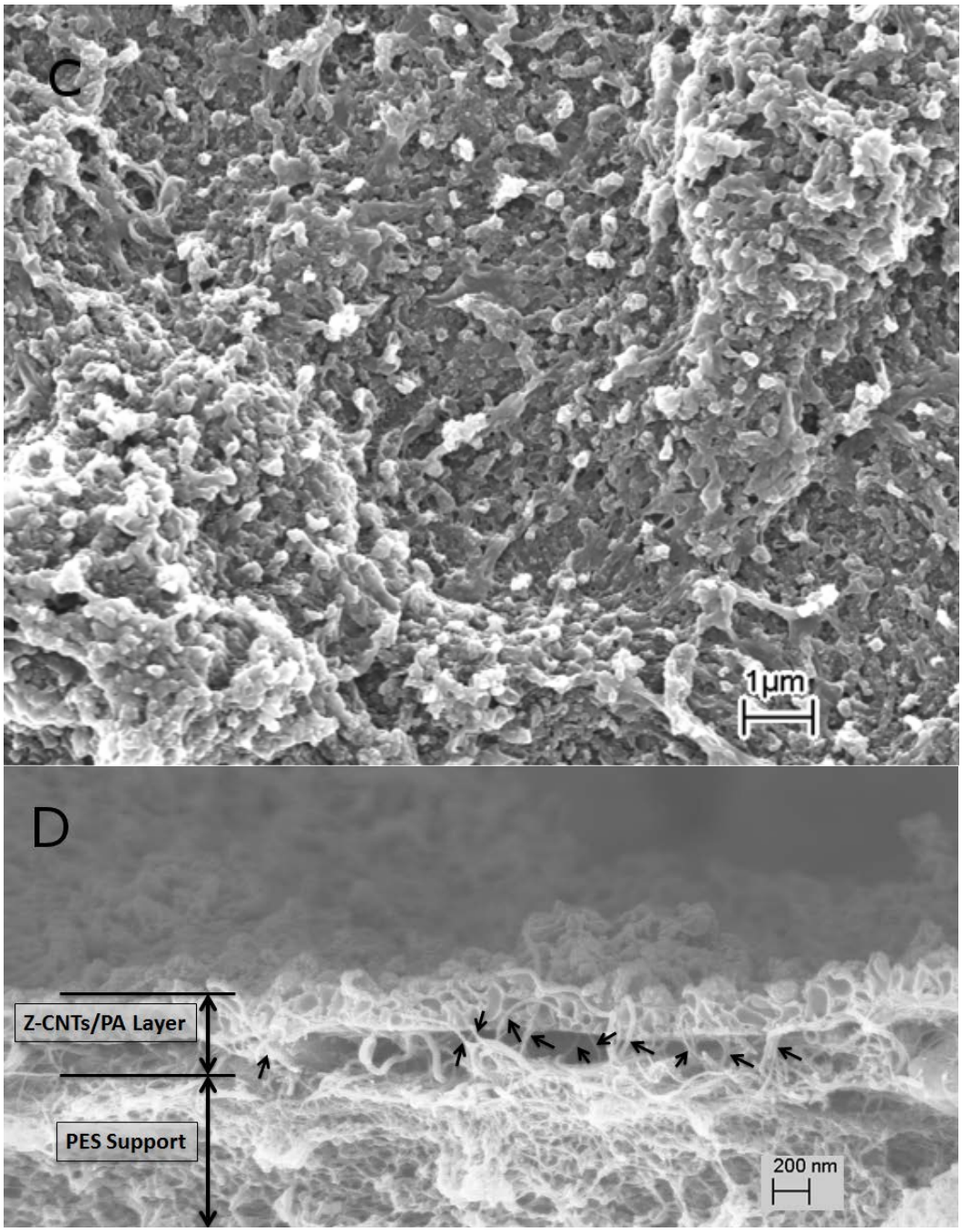

Figure S6. Field emission scanning microscopy images of the PES support and the plain PA and Z-CNTs/PA membranes. The surface morphologies of (A) PES support, (B) PA and (C) Z-CNTs/PA nanocomposite membranes. (D) shows the cross-sectional view of a Z-CNTs/PA membrane.

References

1. Ghosh, A. K.; Hoek, E. M. V., Impacts of support membrane structure and chemistry on polyamide-polysulfone interfacial composite membranes. *J. Membr. Sci.* 2009, 336, 140-148.
2. Saha, N. K.; Joshi, S. V., Performance evaluation of thin film composite polyamide nanofiltration membrane with variation in monomer type. *J. Membr. Sci.* 2009, 342, 60-69.
3. Kong, C.; Kanezashi, M.; Yamomoto, T.; Shintani, T.; Tsuru, T., Controlled synthesis of high performance polyamide membrane with thin dense layer for water desalination. *J. Membr. Sci.* 2010, 362, 76-80.
4. Xie, W.; Geise, G. M.; Freeman, B. D.; S., L. H.; Byun, G.; Mcgrath, J. E., Polyamide interfacial composite membranes prepared from m-phenylene diamine, trimesoyl chloride and a new disulfonated diamine. *J. Membr. Sci.* 2012, 403-404, 152-161.
5. Kim, S.; Jinschek, J. R.; Chen, H.; Sholl, D. S.; Marand, E., Scalable fabrication of carbon nanotube/polymer nanocomposite membranes for high flux transport. *Nano Lett.* 2007, 7, 2806-2811.
6. Zhao, J.; Wang, Z.; Wang, J.; Wang, S., Influence of heat-treatment on CO2 separation performance of novel fixed carrier composite membranes prepared by interfacial polymerization. *J. Membr. Sci.* 2006, 283, 346-356.
7. Ghosh, A. K.; Jeong, B.-H.; Huang, X.; Hoek, E. M. V., Impacts of reaction and curing conditions on polyamide composite reverse osmosis membrane properties. *J. Membr. Sci.* 2008, 311, 34-45.
8. Perdew, J. P.; Burke, K.; Ernzerhof, M., Generalized Gradient Approximation Made Simple. *Phys. Rev. Lett.* 1996, 77, 3865-3868.
9. Kresse, G.; Furthmüller, J., efficient iterative scheme for ab initio total energy calculations using a plane wave basis set. *Phys. Rev. B* 1996, 54, 11169-11186.
10. Kresse, G.; Furthmüller, J., Efficiency of ab initio total energy calculations for metals and semiconductors using a plane wave basis set. *Comput. Mater. Sci.* 1996, 6, 15-50.
11. Kresse, G.; Hafner, J., ab initio molecular dynamics simulations of the liquid metal amorphous semiconductor transition in germanium. *Phys. Rev. B* 1994, 49, 14251-14269.
12. Kresse, G.; Hafner, J., ab initio molecular dynamics for liquid metals. *Phys. Rev. B* 1993, 47, 558-561.
13. Chen, D. L.; Stern, A. C.; Space, B.; Johnson, J. K., Atomic Charges Derived from Electrostatic Potentials for Molecular and Periodic Systems. *J. Phys. Chem. A* 2010, 114, 10225-10233.
14. Corry, B., Designing carbon nanotube membranes for efficient water desalination. *Journal of Physical Chemistry B* 2008, 112, 1427-1434.
15. Alexiadis, A.; Kassinos, S., Molecular Simulation of Water in Carbon Nanotubes. *Chem. Rev.* 2008, 108, 5014-5034.